J. Synchrotron Rad. (1998). **5**, 286–292

Experiments with Very High Energy Synchrotron Radiation

Th. Tschentscher* and P. Suortti

European Synchrotron Radiation Facility, BP 220, F-38043 Grenoble CEDEX 9, France. E-mail: thomas.tschentscher@desy.de

(*Received 4 August 1997; accepted 28 October 1997*)

The use of synchrotron radiation with very high photon energies has become possible only with the latest generation of storage rings. All high-electron-energy synchrotron sources will have a dedicated program for the use of very high photon energies. The high-energy beamline ID15 at the ESRF was the first beamline built and dedicated to this purpose, and it has now been in user operation for more than three years. The useful energy range of this beamline is 30–1000 keV and the superconducting insertion device for producing the highest attainable photon energies is described in detail. The techniques most often used today are diffraction and Compton scattering; an overview of the most important experiments is given. Both techniques have been used in the investigation of magnetic systems, and, additionally, the high resolution in reciprocal space, which can be achieved in diffraction, has led to a series of applications. Other fields of research are addressed, and attempts to indicate possible future research areas of high-energy synchrotron radiation are made.

Keywords: high-energy synchrotron radiation; bent crystals; magnetic Compton scattering; reciprocal-space mapping; non-resonant magnetic scattering.

1. Introduction

The use of very high photon energies provided by synchrotron radiation has become possible only recently due to the advent of high-electron-energy storage rings like the ESRF, APS and SPring-8. Experiments with high-energy photons had already demonstrated that high-energy diffraction (Hastings *et al.*, 1989), Compton scattering or scattering from amorphous samples (Poulsen *et al.*, 1994) would largely benefit from an increase in the primary photon energy. Dedicated sources with high flux provide the possibilities to perform spectroscopy experiments at the K-edge of high-Z materials, *e.g.* 115.6 keV for U, and materials investigations benefit from less absorption, probing therefore the bulk and facilitating the sample environment. In nuclear resonance scattering the excitation of new atoms with higher nuclear levels becomes possible. Development of dedicated optical components allows focusing in the micrometre range to be achieved, even for energies of ~100 keV. The high-energy beamline ID15 at the ESRF became operational in 1994 and since then more than 100 user experiments have been performed. Experiments often require good counting statistics and therefore simultaneous operation of three stations was foreseen. Two insertion devices with high critical energies, E_c, both providing circular-polarized photons using an inclined-view method, are available. The multipurpose layout of the beamline enables experiments with varying techniques in the energy range 30–1000 keV, and the layout of the optics is chosen to be versatile enough to provide high flexibility for new experimental techniques. Experiments split about equally into high-energy diffraction and inelastic Compton scattering studies and a third of the time is used for varying techniques and optics development. This paper provides a brief summary of the status of the beamline and the major achievements during the past years. The superconducting insertion device is described and the optimization of the optical components is reviewed. The experimental techniques most often used will be introduced and explained in more detail using results from performed experiments.

2. High-energy beamline at the ESRF

2.1. *Insertion devices and beamline layout*

The asymmetric multipole wiggler (AMPW) with E_c = 45 keV at a magnetic gap of 20 mm serves the highest flux for all experiments up to an energy of ~150 keV. The seven strong poles produce a beam with a full width of 4.4 mrad and a total power of 6.5 kW at a storage ring current of 100 mA. This device is complemented by a superconducting insertion device, called a superconducting wavelength shifter (SCWS), which contains one strong pole with a magnetic field of 4 T and two weak poles of 1.3 T. The total length of the device, installed 2 m downstream of the AMPW, is 500 mm and the superconducting coils generating the magnetic field are He-cooled. The coils are made from conventional superconducting wire and are kept at a temperature of 4.4 K by means of a 200 l

liquid-He bath cryostat. The evaporating He is re-liquefied by a two-stage closed-cycle cooling system, thus avoiding He losses and reducing the maintenance of the system to a minimum. The cryostat is constructed in such a way that the vacuum chamber for the electron beam is kept at room temperature. The SCWS has a critical energy E_c of 96 keV and generates a 12.6 mrad-wide fan with a total power of only 5.1 kW. Fig. 1 shows the flux distribution for both insertion devices as a function of energy. The low-energy part of the spectrum is filtered by means of a permanently installed cooled Al absorber with a thickness of 4 mm, and horizontally the beams are confined by 60 mm-thick W blocks into three radiation fans of widths 0.8, 1.2 and 1.0 mrad. The horizontal definition of the beams protects heatload-sensitive structures and allows for the independent operation of different stations. The two insertion devices are used alternately due to the limitation of total power in the front end, except in the so-called 16-bunch filling mode for which the reduced stored electron current can be partially compensated by running both insertion devices simultaneously.

The beamline features three experimental stations each equipped with slits, beam-position monitors and beam shutters to enable independent operation. The experiments are scheduled on the high-energy diffraction beamline ID15A, comprising the experimental stations B and P, and the high-energy inelastic-scattering beamline ID15B with the experimental station S (Suortti & Tschentscher, 1995). The in-vacuum monochromators for stations P and S are at 38 and 42 m from the AMPW, respectively. The monochromators are installed on longitudinal and transverse translation stages, which allow for ±5% tuning of the energy. A vertical translation gives access to different monochromator crystals and therefore different energy bands in the fixed-angle geometry. Bent Si crystals are employed as monochromators, which are transparent for further use of the beam by the downstream instruments. The main instrument at station S is a scanning spectrometer dedicated to Compton scattering, and the monochromators are mounted in focusing Bragg geometry providing 2×10^{12} photons s^{-1} $(100\ mA)^{-1}$ in a bandwidth of 4×10^{-4} at an energy of 60 keV. The focal width is ∼0.5 mm and optimal conditions for high-resolution Compton spectroscopy with resolution down to 0.08 a.u. are obtained (Suortti, Buslaps *et al.*, 1998). The energy range for this instrument spans from 30 to 60 keV, with the possibility of using the second harmonics of Si 220 at 100 keV. The monochromator for station P is chosen to be very flexible in order to make possible a wide range of experiments with different monochromatization requirements. It can be used in Laue or Bragg geometry and the direction of bending can be changed, thus enabling an energy-resolving inverse Cauchois geometry or a focusing geometry accompanied by a wide energy band (Suortti, Lienert & Schulze, 1997). The station is mainly dedicated to diffraction experiments in the energy range 30–100 keV. It has been very valuable in the preparation of experiments, when tests, *e.g.* of crystal mosaicity, had to be performed under similar conditions as the experiment. Tests of varying optical components can be performed easily due to the high flexibility of the station.

End-station B allows the use of either a white or monochromatic beam. The use of a white beam arises mainly from the permanently installed triple-crystal diffractometer for reciprocal-space mapping. To maintain the intrinsic high resolution of this instrument, all axes must have very precise angular encoding. Despite the disadvantage of higher scattering background, the monochromatization is performed on the instrument itself, and an optical interferometer simultaneously encodes all axes. Other white-beam experiments, like powder diffraction or single-crystal diffraction, have been carried out with variable set-ups. For a monochromatic beam the monochromator is mounted on an optical table at ∼60 m from the AMPW in a small optics hutch. Thus, the mounting is facilitated and background scattering in the experimental hutch is largely suppressed. Due to the varying needs of a monochromatic beam with energies from 30 to 1000 keV, bandwidths from 1×10^{-5} to 1×10^{-1} and beam sizes from 10×10 μm to 50×10 mm, a variety of monochromators are available. In experiments using circular-polarized photons the beam is vertically limited by slits blocking the linearly polarized photons emitted in the plane of the storage ring and giving access to the circular-polarized photons either above or below the beam centre. In Fig. 1 the available flux for different degrees of linear and circular polarization is shown for both insertion devices. Other methods of producing circular-polarized photons, like elliptical wigglers (Yamamoto *et al.*, 1989) or phase-retarding crystals (Lang *et al.*, 1996), may not yield the same flux at high energies. In addition, their use would penalize part of the beamline during the simultaneous operation or give too narrow energy bands.

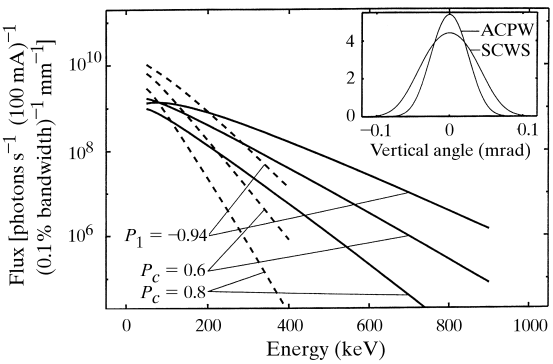

Figure 1
Flux for SCWS (solid lines) and AMPW (broken lines) as a function of energy. Vertically the beam is integrated to obtain a polarization state described by its average Stokes parameter P_l and P_c for linear- and circular-polarized photons, respectively. The inset shows the vertical brightness distribution for both insertion devices at E = 200 keV.

2.2. *Monochromators*

Most optical components employ bent-crystal Si monochromators, which are well suited for use with high-energy photons and versatile enough to be adapted to the needs of different experimental techniques. These monochromators can provide focusing, an increased energy and angular acceptance and do not affect the circular polarization of the beam if used in horizontal scattering geometry. Reflection curves can be adapted to the experiment in a controlled way *via* bending. The theory of bent-crystal monochromators for synchrotron radiation has been introduced (see *e.g.* Suortti & Freund, 1989), and only a brief summary is given here. The energy band of a beam monochromated by reflection at a Bragg angle θ is generally described by $\Delta E/E = \cot\theta\,\Delta\theta$ due to the varying orientation of lattice planes with respect to the incident white beam. For perfect flat-crystal monochromators, the integrated reflectivity is limited by the Darwin width, $\omega_{\rm D} = 2d/(\pi\cos\theta\,\Lambda)$ of the reflection curve, but the extinction length, Λ, increases at high energies and the angular acceptance of a reflection with lattice spacing d becomes much smaller than the source divergence. Bending the crystal meridionally introduces a well defined disorder of the crystal planes, which widens the reflection curve without loss in the maximum reflectivity. If the bending changes the orientation of the crystal planes by more than $\omega_{\rm D}$ over a distance equal to the extinction length, the crystal starts to reflect kinematically and the peak reflectivity increases to 100% (Schulze & Chapman, 1995). Further bending will broaden the reflection curve and thus increase the integrated reflectivity. Once the kinematical limit for the integrated reflectivity is reached, an increase in bending will continue broadening of the reflection curve, but decrease the maximum reflectivity. Monochromatic and polychromatic focusing geometries are possible for single-crystal monochromators. Monochromatic focusing can be achieved only in Bragg geometry where source and image lie on the Rowland circle of radius $\rho/2$, with the distances $p_0 = \rho\cos(\chi \pm \theta)$ and $q_0 = \rho\cos(\chi \mp \theta)$, respectively. Here, ρ is the bending radius of the crystal and χ is the asymmetry of the Bragg planes. The upper and lower sign have to be applied for magnifying and demagnifying geometry, respectively. In Laue geometry the image on the Rowland circle is virtual, but the transmitted beam is reflected without energy broadening due to source divergence. Energy broadening on a path through a crystal arises from the different orientation of scattering planes at the front and back surface of the crystal and from elastic deformation. In the case of polychromatic focusing, neither source nor focus lie on the Rowland circle and it is possible to use Laue geometry in focusing applications. A widened energy band, $\Delta E/E = \cot\theta\, h(1/p_0 - 1/p)$, is obtained with respect to the width, h, of the beam for the source distance $p = p_0/(2 - q_0/q)$ and the focal distance q. The focus size is generally limited by the fact that the geometrical focus has to coincide with the polychromatic focus for an infinitely small beam (Schulze *et al.*, 1998). It was shown recently that even micrometre focusing at photon energies around 80 keV is possible in this geometry (Lienert *et al.*, 1998). In the case of bent-crystal double monochromators, the focus point of the first crystal serves as the source point for the second crystal.

For inelastic scattering it is important to tailor a monochromatic beam which provides the highest possible flux for linear- or circular-polarized photons and a band pass of the incident beam which does not decrease the experimental resolution. Single-bounce monochromators in horizontal scattering geometry are chosen, and experiments are performed at scattering angles close to 170° using energy-dispersive Ge detectors for the detection of the scattered photons. The resolution due to geometrical broadening is very small and the energy resolution of the detector gives the main contribution to the resolution function. The component due to the band pass of the incident beam needs to be adapted to the experiment to achieve maximum intensity. Generally, the bandwidth increases with the cotangents of the Bragg angle θ, but the band is partially compensated due to the large energy shift of the Compton-scattered photons. Typically, bandwidths of 1×10^{-3} to 4×10^{-3} are requested for fixed energies. In experiments with low-energy resolution the bandwidth has been increased to 10^{-1}, gaining a factor of ten in flux. For studies of heavy-material K-edges a resolution of 1×10^{-4} is needed in conjunction with the possibility of energy scanning. For the energy range 70–120 keV, a bent-crystal Laue–Bragg monochromator has been developed, where the first crystal reflects in highly asymmetric Laue geometry and the second crystal, mounted in Bragg geometry, focuses the beam onto the sample. For the Si 531 reflection and a 40 mm-wide incident beam, a focus of 400 µm has been obtained at 8 m from the monochromator with a reflectivity of ~25% and a bandwidth of $\leq 2 \times 10^{-4}$ (Lienert & Schulze, 1998). For nuclear resonance scattering experiments an energy resolution of 1×10^{-5} and better is necessary, which cannot be achieved with the present insertion devices in horizontal scattering geometry due to the source divergence. A vertically reflecting bent-crystal double Laue monochromator has been designed and in first tests an energy resolution of 4×10^{-5} with a photon flux of 1×10^{8} photons $\rm s^{-1}\,mm^{-2}\,(100\,mA)^{-1}$ could be achieved for the Si 311 reflection. Inverse Cauchois geometry with a bending radius of 60 m is employed, and the energy band is defined by the vertical source size $\sigma_{v,\rm r.m.s.} = 11$ µm, the thickness and asymmetry of the first crystal. High-precision rotation stages have to be used to achieve the requested angular resolution.

2.3. *Detection*

Detection of high-energy photons is generally limited by a decreasing absorption due to the photo-effect. Absorption by Compton scattering can strongly contribute to the total absorption, but only part of this energy is deposited within the detector volume. This becomes especially

important for the detection of photon energies. A simulation for Ge detectors used for inelastic scattering showed that the efficiency of detecting photons of certain energy follows almost the absorption due to the photo-effect (Fajardo *et al.*, 1998). In diffraction experiments, energy resolution is beneficial to suppress background and higher-order reflections, but, in contrast to inelastic scattering, high resolution is not needed. Therefore, thicker Ge crystals can be used, increasing the efficiency (Fig. 2). The time resolution of a Ge detector is limited by the charge collection to a few nanoseconds, but, recently, avalanche photodiodes have been used in time-resolving diffraction experiments (Liss, Magerl, Hock *et al.*, 1997), where high count rates can be achieved, and a time resolution of ~800 ps was obtained. Two-dimensional detectors must have efficient converters of X-ray photons to light which also maintain the spatial resolution. A resolution of 100 μm could be expected for 80 μm-thick screens of the type used for CCD cameras or image plates. The use of two-dimensional detectors can improve diffraction experiments in many ways and may be particularly interesting in studies of diffuse scattering, where no high spatial resolution is needed. For inelastic scattering experiments, spatial resolution is generally not needed, but due to the count-rate limitation the use of multipixel detectors would increase the total count rate.

3. High-energy diffraction

Most diffraction experiments utilize the triple-crystal diffractometer (TCD) with horizontal scattering geometry, which is installed at station B for use with energies covering the whole spectrum. These instruments have shown to be versatile in studies of structure factors of amorphous materials, crystal structure and properties, structural phase transitions and antiferromagnetism with high-energy synchrotron radiation (Schneider *et al.*, 1994). The three axes of the TCD are mounted on an optical table and an additional table serves for the translation of the energy-dispersive Ge detector. The beam is monochromated by the first crystal and appropriate rotations of sample and analyser crystal enable mapping of reciprocal space. The instrument therefore combines the possibility of measuring lattice plane orientations and lattice parameters at the same time. Typically, monochromator and analyser crystals are similar and a non-dispersive scattering geometry is chosen where the lattice spacings of all three crystals are equal or at least very close to each other (Neumann *et al.*, 1994; Rütt *et al.*, 1995). In the case of perfect crystals, a transverse resolution of 0.9×10^{-6} and a longitudinal resolution of 6.2×10^{-6} are achieved for the Si 531 reflection at 150 keV. The third resolution component perpendicular to the scattering plane is determined by the height of the beam, the distance and vertical acceptance of the detector. When samples with increased mosaicity are investigated or higher throughput is needed, the monochromator and analyser are replaced by Si or Ge crystals with intrinsic mosaicity and no angular encoding is needed. The latter case is applied typically for industrial samples or in the investigation of non-resonant magnetic diffraction.

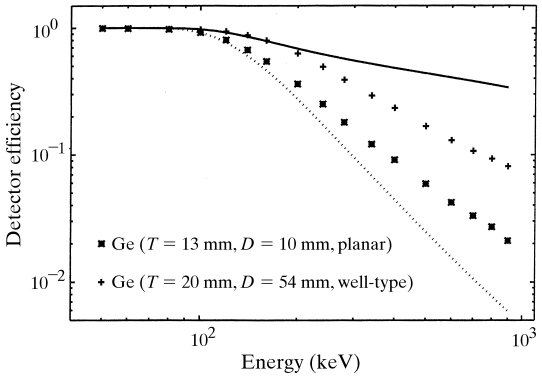

Figure 2
Detection efficiency for high-energy synchrotron radiation from a Monte Carlo calculation for Ge detectors with thicknesses T and diameters D as a function of energy. The impinging beam is 6 mm in diameter and the lines indicate total absorption (solid) and absorption due to the photo-effect (dotted) for the planar detector, frequently used for energies up to 150 keV.

3.1. *High-resolution diffraction*

Distortion of the lattice in gradient crystals can lead to an increase in the integrated reflectivity. In addition, the coherence of the diffracted beam is preserved and gradients can be realized by temperature, composition or ultrasound. To investigate ultrasonic excitation of perfect Si crystals, a transducer is bonded to the [111] surface, and, when a resonance frequency of ~5 MHz is applied, a standing wavefield is created in the crystal. A scattering plane has been chosen almost perpendicular to the [111] direction and the crystal was investigated in non-dispersive geometry. It is observed that the ultrasonic excitation generates a distortion of the lattice only in the [111] direction and that the amplitude of this distortion relates to the amplitude of the exciting field. In Fig. 3, reflection curves are shown and one observes how the integrated intensity increases with the control voltage until the kinematical diffraction limit starts to decrease the maximum reflectivity, whereas the width of the reflection curves continuously increases (Liss, Magerl, Remhof *et al.*, 1997). An intensity gain of 50 compared with the perfect crystal was achieved.

High-resolution diffraction is also needed when very small changes of lattice parameters, *e.g.* at phase transitions, shall be followed. The rare-earth system $EuAs_3$ has a commensurate–incommensurate lock-in phase transition at T_L = 10.3 K, and, when the lattice parameter was measured as a function of temperature, an anomaly in the thermal expansion due to magneto-elastic effects was obtained at T_L (Chattopadhyay *et al.*, 1997). The observed variation is of the order of 5×10^{-5} and an instrument resolution of 6×10^{-6} is essential. The lattice parameter variation has been observed at a charge reflection, whereas

pure magnetic scattering can be observed from the same crystal at charge forbidden reflections.

3.2. *Non-resonant magnetic scattering*

The amplitude of weak scattering processes, like magnetic scattering in comparison with charge scattering, is enhanced when high photon energies are used and the probed volume increases correspondingly. Because the magnetic scattering is small, only reflections for which charge scattering is forbidden can be used. Experiments have therefore concentrated on antiferromagnetically ordering crystals with reasonable mosaicity and broad-band monochromators are employed. Non-resonant magnetic diffraction arises as a second-order term in the cross section for diffraction (de Bergevin & Brunel, 1981; Blume & Gibbs, 1988), and for high photon energies with very small scattering angles it is sensitive to the electron spin moment only. The validity of the cross section for photon energies up to 500 keV and the expected $\cos^2$ dependence for the spin orientation have been verified recently, indicating that no additional scattering occurs at high energies (Strempfer *et al.*, 1997). With these results it becomes possible to determine from the scattered intensity the spin magnetization. Non-resonant magnetic scattering can therefore probe magnetic moments in the bulk and has a great potential for the study of magnetism in materials with zero or small resonance enhancement, like 3*d* or 4*d* transition metals and rare-earth materials.

The model system MnF_2 had been investigated in a first experiment at a photon energy of 80 keV (Strempfer *et al.*, 1996), and recently a second experiment used energies in the range 100–500 keV. At 80 keV, peak intensities of 13000 photons s^{-1} have been observed in the three-crystal mode and 19000 photons s^{-1} in two-crystal mode, with peak-to-background ratios of 230:1 and 10:1, respectively. In the semi-metallic rare-earth system $EuAs_3$ (Chattopadhyay *et al.*, 1988), measurements at a photon energy of 104 keV achieved intensities of 200 photons s^{-1} and peak-to-background ratios of 10:1 in the three-crystal mode. The strength of the magnetic signal is reduced due to higher absorption and smaller magnetization. In addition, the mosaicity of the sample is rather large. The temperature dependence of the magnetic (3, 0, 3/2) reflection was followed, and, below the transition temperature T_L = 10.3 K for the lock-in transition from the incommensurate sine wave phase to the commensurate antiferromagnetic phase, the sublattice formation could be studied. The intensities of several magnetic reflections have been determined and the values have been compared with a magnetic structure model. The overall agreement indicates the possibility of calculating magnetic structures on the basis of diffraction data observed by non-resonant magnetic scattering with high-energy radiation.

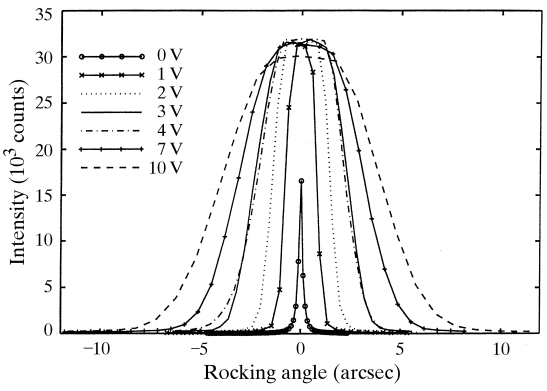

Figure 3
Reflection curves of the Si 531 reflection for different control voltages of the ultrasonic wave field measured at 90 keV. The ultrasonic excitation took place along the [111] direction almost perpendicular to the scattering vector.

3.3. *Materials investigation*

In the microstructural investigation of materials, the use of TCD techniques at high energies provides the possibility of investigating non-destructively the bulk of samples (thicknesses = 10 mm) with respect to strain and lattice orientation. Additionally, the use of furnaces is facilitated due to smaller absorption, and identical samples as used in neutron studies can be investigated. The achieved q resolution is typically one order of magnitude better than in neutron measurements, and very small lateral dimensions of 10 × 10 μm can be probed. In a series of experiments on single-crystal Ni-based superalloys, the evolution of the lattice mismatch between the two phases γ and γ' was investigated as a function of the thermomechanical history of the sample (Royer & Bastie, 1997). Due to the instrument resolution the reflection curves could be analysed in terms of distinct phases, which could be followed during the temperature cycle. In addition, it was possible to measure weak superstructure reflections, which provide more specific information about single phases (Royer *et al.*, 1997).

4. Inelastic scattering

4.1. *Magnetic Compton scattering*

In magnetic Compton scattering the spin density distribution of ferro- and ferrimagnets is investigated by Compton scattering using circularly polarized photons. Due to the circular polarization, additional scattering arises from the magnetic spin moment of the electrons, which can be obtained as the difference between two spectra, when either the helicity of the photon or the magnetization of the sample is inverted. Both methods have been tried, but only the latter has been found practical, due to the difficulty in monitoring accurately the ratio of circular- to linear-polarized photons at these energies. A series of experiments for different incident energies showed that the use of photon energies around 200–250 keV provides optimal experimental conditions with an improved momentum resolution of ∼0.37 a.u. and an increase of the magnetic signal by a factor of two compared with earlier experiments at photon energies of

60 keV. Experiments have been carried out for photon energies from 100 to 1000 keV on various samples and momentum distributions and the total partial magnetic spin moments have been investigated (Tschentscher *et al.*, 1998). Fig. 4 shows, as an example, the magnetic Compton profile from $CeRh_3B_2$ with antiferromagnetic coupling of all spins. The shape of the distribution indicates which electrons contribute to the total magnetic moment (Yaouanc *et al.*, 1998).

4.2. *(γ,eγ) coincidence experiments*

In highly inelastic scattering experiments the coincident detection of a Compton scattered photon and its recoil electron allows for the determination of the complete three-dimensional electron momentum distribution (EMD) of a solid-state target. To avoid multiple scattering of the recoil electron within the target, very thin foils have to be used. At an incident photon energy of 150 keV and a scattering angle $\theta = 140^\circ$ for the photon, the electron escapes with an energy of ~50 keV. In a series of measurements the three-dimensional momentum distribution in pyrolitic graphite has been investigated (Kurp *et al.*, 1996), and recently a 256-pixel electron detector was installed and could be used for the first time in experiments on Cu–Ni alloys. The total coincidence rate could be increased and the feasibility of measurements with improved resolution in all three dimensions ($\Delta p_x =$ 0.25 a.u., $\Delta p_y =$ 0.36 a.u., $\Delta p_z =$ 0.52 a.u.) was demonstrated. Measurements of similar samples before and after heat-induced diffusion provided a higher sensitivity for changes of the EMD due to the alloying process. These results will be published separately.

4.3. *Cross section for double ionization of He*

Calculations of the cross section ratio for double ionization, $R_C = \sigma^{++}/\sigma^{+}$, of He by Compton scattering are highly sensitive to electron correlation in the initial and final state and give an asymptotic value for increasing energy. Different theories disagree, and the experiments were intended to provide experimental evidence. Experiments have been carried out at 60 and 100 keV and it was requested to provide as much flux as possible due to the very small scattering cross section. The experiments are performed using an He gas jet and electrons and double-ionized recoil ions are detected in coincidence. A bent Laue crystal monochromator had been chosen, which focused a 40 mm beam to 1 mm in a bandwidth of 1×10^{-1} (Spielberger *et al.*, 1996; Wehlitz *et al.*, 1996). It is foreseen to extend these measurements to even higher photon energies to confirm the asymptotic behaviour.

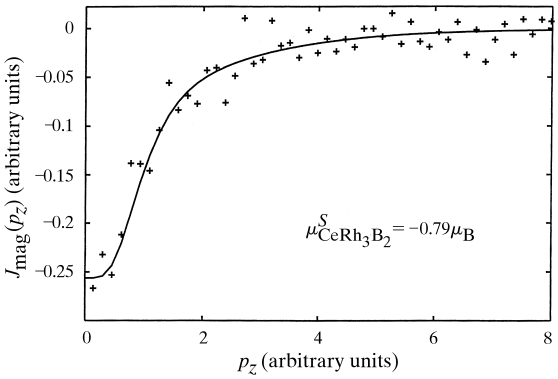

Figure 4
Magnetic Compton profile for the ternary boride $CeRh_3B_2$ at $T =$ 9 K. The scattering angle was 172° and an external field of 0.92 T was switched in periods of 100 s to obtain the difference profile. $\mu^S_{CeRh_3B_2}$ is the total spin magnetization of the system as obtained from the experiment. The solid line indicates a fit of atomic profiles for Ce(4*f*), Ce(5*d*) and Rh(4*d*) to the data.

5. Other experiments and future trends

In measurements of the scattering function, $S(Q)$, for amorphous SiO_2 and GeO_2 it could be shown that the use of high-energy photons is highly beneficial, and that high accuracy of the data can be achieved. The experiments have been carried out in angle-dispersive geometry using the TCD for sample mount and detector. The incident beam was monochromated by means of a bent crystal with wide band pass optimized with respect to the instrument resolution. The monochromator was mounted in the upstream hutch to suppress background, and scanning of the detector with defining slits has served for the 2θ determination (Neuefeind & Liss, 1996). Energy-dispersive experiments have been carried out using white beam, where the low-energy part of the spectrum is absorbed by filters and upstream monochromators. Powder diffraction and single-crystal diffraction were used in the verification of source parameters and in the investigation of thermal diffuse scattering, respectively. Energy-dispersive diffraction at high photon energies is a technique well suited for experiments with high-pressure cells, and the fast data accumulation provides the possibility of following *in situ* processes of the sample.

X-ray interferometry at high photon energies provides high accuracy in the determination of atomic scattering factors. In two experiments the scattering amplitudes from Ta, W, Pt, Au and Pb at the respective *K*-edges, and the relativistic corrections for Si, CaF_2, Ge, Ag and Sn, have been measured. The mounting of the single-crystal interferometer on the monochromator axis of the TCD showed very good stability and interference patterns were obtained for energies up to 540 keV (Lienert *et al.*, 1997). The use of very high photon energies is important in the determination of the relativistic correction, because the requested accuracy demands measurements far away from the *K*-edges.

In nuclear resonance scattering, hyperfine interactions of atoms in crystal fields can be detected. Experiments with synchrotron radiation are concentrating on the energy range $\lesssim$30 keV, but the excitation of resonances at energies of 60 keV and higher has been frequently suggested. To limit electronic scattering background, fixed-exit monochromators have to be employed which provide

the highest possible resolution but maintain maximum reflectivity in the same time. A double-crystal bent-Laue monochromator was built for vertical diffraction geometry in order to benefit from the smaller vertical divergence of the synchrotron beam. To achieve the necessary resolution and stability for energy scanning, further improvement of the monochromator will be needed.

6. Conclusion and outlook

Operations at the high-energy beamline at the ESRF have shown during the past three years that many experiments benefit from the use of high-energy photons. Especially in studies of magnetism by non-resonant diffraction and magnetic Compton scattering, high-quality results could be obtained. The high resolution in reciprocal-space mapping provides the possibility of investigating small distortions or changes in the lattice constants, *e.g.* at phase transitions, and the *in situ* investigation of thick materials becomes possible. To increase the field of applications in the future, the angular resolution of the TCD will be improved and a cryomagnet shall give access to materials with very small magnetization in Compton scattering and diffraction. A multi-element Ge detector will be very beneficial for increasing the total count rate in inelastic scattering, and high-resolution Compton spectroscopy shall be extended to an energy of ~100 keV by means of analyser crystals in Laue geometry. Other fields like the determination of structure factors in amorphous materials or nuclear resonance scattering at photon energies around and above 100 keV will become more important and the optics development program is to be continued to enable the realization of new ideas in the future.

We would like to acknowledge all colleagues who let us show their results in this paper, some even prior to publication. The help of V. Honkimäki during many experiments and with the data treatment is highly appreciated. We thank P. Fajardo for the provision of the Monte Carlo code for the detector efficiency. The Laue–Bragg monochromator has been developed in close collaboration with U. Lienert and C. Schulze. The magnet used in the magnetic Compton studies was supplied by the University of Warwick.

References

Bergevin, F. de & Brunel, M. (1981). *Acta Cryst.* A**37**, 314–324.
Blume, M. & Gibbs, D. (1988). *Phys. Rev. B*, **37**, 1779–1789.
Chattopadhyay, T., Brown, P. J., Thalmeier, P., Bauhofer, W. & von Schnering, H. G. (1988). *Phys. Rev. B*, **37**, 269–282.
Chattopadhyay, T., Liss, K.-D. & Tschentscher, Th. (1997). *Highlights 1996/1997, ESRF, Grenoble*, p. 19.
Fajardo, P., Honkimäki, V., Buslaps, T. & Suortti, P. (1998). *Nucl. Instrum. Methods.* In the press.
Hastings, J. B., Siddons, D. P., Berman, L. E. & Schneider, J. R. (1989). *Rev. Sci. Instrum.* **60**, 2398–2401.
Kurp, F. F., Tschentscher, Th., Schulte-Schrepping, H., Schneider, J. R. & Bell, F. (1996). *Europhys. Lett.* **35**, 61–66.
Lang, J. C., Srajer, G. & Dejus, R. J. (1996). *Rev. Sci. Instrum.* **67**, 62–67.
Lienert, U., Hart, M., Laundy, D. & Liss, K.-D. (1997). *Highlights 1996/1997, ESRF, Grenoble*, pp. 88–90.
Lienert, U. & Schulze, C. (1998). To be published.
Lienert, U., Schulze, C., Honkimäki, V., Tschentscher, Th., Garbe, S., Hignette, O., Horsewell, A., Lingham, M., Poulsen, H. F., Thomsen, N. B. & Ziegler, E. (1998). *J. Synchrotron Rad.* **5**, 226–231.
Liss, K.-D., Magerl, A., Hock, R., Remhof, A. & Waibel, B. (1997). *Europhys. Lett.* **40**, 369–374.
Liss, K.-D., Magerl, A., Remhof, A. & Hock, R. (1997). *Acta Cryst.* A**53**, 181–186.
Neuefeind, J. & Liss, K.-D. (1996). *Ber. Bunsenges. Phys. Chem.* **100**, 1341–1349.
Neumann, H.-B., Rütt, U., Bouchard, R., Schneider, J. R. & Nagasawa, H. (1994). *J. Appl. Cryst.* **27**, 1030–1038.
Poulsen, H. F., Neuefeind, J., Neumann, H.-B., Schneider, J. R. & Zeidler, M. D. (1994). *J. Non-Cryst. Solids*, **188**, 63–74.
Royer, A. & Bastie, P. (1997). *Scr. Mater.* **36**, 1051–1159.
Royer, A., Bastie, P. & Vernon, M. (1997). *Mater. Sci. Eng. A*, **234–236**, 1110–1113.
Rütt, U., Neumann, H.-B., Poulsen, H. F. & Schneider, J. R. (1995). *J. Appl. Cryst.* **28**, 729–737.
Schneider, J. R., Bouchard, R., Brückel, T., Lippert, M., Neumann, H.-B., Poulsen, H. F., Rütt, U., Schmidt, T. & von Zimmermann, M. (1994). *J. Phys. IV*, C**9**, 415–421.
Schulze, C. & Chapman, D. (1995). *Rev. Sci. Instrum.* **66**, 2220–2223.
Schulze, C., Lienert, U., Hanfland, M., Lorenzen, M. & Zontone, F. (1998). *J. Synchrotron Rad.* **5**, 77–81.
Spielberger, L., Jagutzki, O., Krässig, B., Meyer, U., Khayyat, Kh., Mergel, V., Tschentscher, Th., Buslaps, T., Bräuning, H., Dörner, R., Vogt, T., Achler, M., Ullrich, J., Gemmell, D. S. & Schmidt-Böcking, H. (1996). *Phys. Rev. Lett.* **76**, 4685–4688.
Strempfer, J., Brückel, T., Hupfeld, D., Schneider, J. R., Liss, K.-D. & Tschentscher, Th. (1997). *Europhys. Lett.* **40**, 569–574.
Strempfer, J., Brückel, T., Rütt, U., Schneider, J. R., Liss, K.-D. & Tschentscher, Th. (1996). *Acta Cryst.* A**52**, 438–449.
Suortti, P., Buslaps, Th., Fajardo, P., Honkimäki, V., Kretzschmer, M., Lienert, U., McCarthy, J. E., Renier, M., Shukla, A., Tschentscher, Th. & Meinander, T. (1997). To be published.
Suortti, P. & Freund, A. (1989). *Rev. Sci. Instrum.* **60**, 2579–2585.
Suortti, P., Lienert, U. & Schulze, C. (1997). *X-ray and Inner-Shell Processes, 17th International Conference. AIP Conference Proceedings 389*, edited by R. L. Johnson, H. Schmidt-Böcking & B. F. Sonntag, pp. 175–192. New York: Woodbury.
Suortti, P. & Tschentscher, Th. (1995). *Rev. Sci. Instrum.* **66**, 1798–1801.
Tschentscher, Th., McCarthy, J. E., Honkimäki, V. & Suortti, P. (1998). *J. Synchrotron Rad.* **5**, 940–942.
Wehlitz, R., Hentges, R., Prümper, G., Farhat, A., Buslaps, T., Berrah, N., Levin, J. C., Sellin, I. A. & Becker, U. (1996). *Phys. Rev A*, **53**, R3720–R3722.
Yamamoto, S., Shioya, T., Sasaki, S. & Kitamura, H. (1989). *Rev. Sci. Instrum.* **60**, 1834–1837.
Yaouanc, A., Dalmas de Reotier, P., Sanchez, J. P., Tschentscher, Th. & Lejay, P. (1998). *Phys. Rev. B*, **57**, R681–R684.